

Semi-supervised Parametric Real-world Image Harmonization

Ke Wang^{1,2}, Michaël Gharbi¹, He Zhang¹, Zhihao Xia¹, Eli Shechtman¹
¹ Adobe Inc.

² EECS, University of California, Berkeley

{kewang, mgharbi, hezhan, zxia, elishe}@adobe.com

kewang@berkeley.edu

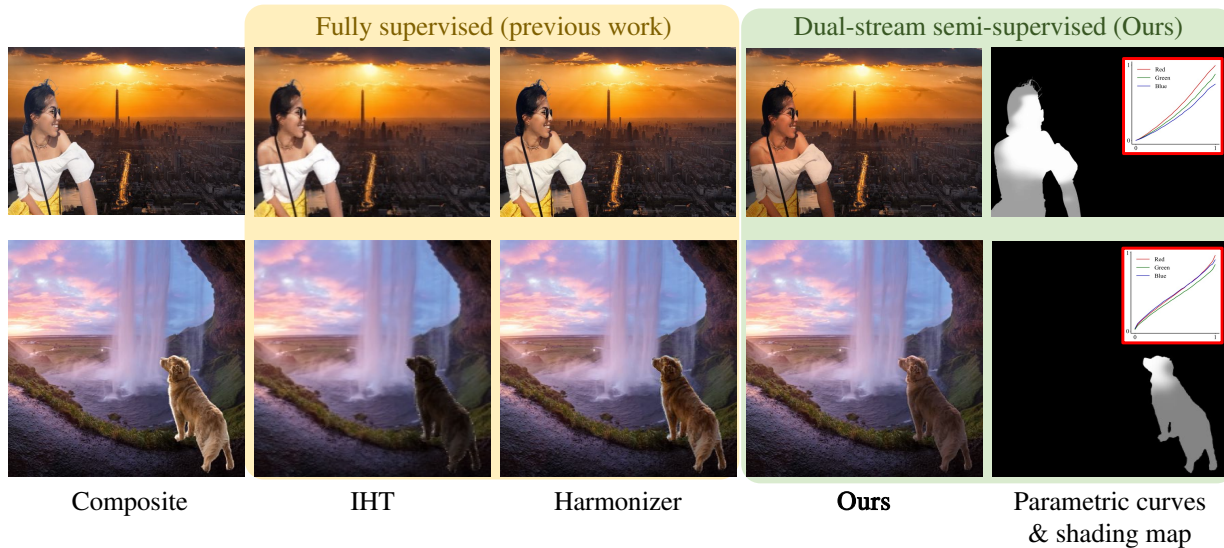


Figure 1. **Visual comparisons between state-of-the-art harmonization methods IHT [9], Harmonizer [14], and ours.** Our model is fully parametric. This gives artists full posterior control over the final composite, makes runtime efficient for high-resolution real-world inputs and regularizes training. Our model predicts *global RGB curves* and a *local shading map* (right). Benefiting from the novel dual-stream semi-supervised training strategy, our method (right) produces more realistic harmonized images on real-world composites (left). This new training strategy, together with the shading map, makes it the first harmonization method to address local tonal adjustments, such as shading the face according to the sun’s direction (top) or selectively darkening the part of the dog inside the cave (bottom).

Abstract

Learning-based image harmonization techniques are usually trained to undo synthetic random global transformations applied to a masked foreground in a single ground truth photo. This simulated data does not model many of the important appearance mismatches (illumination, object boundaries, etc.) between foreground and background in real composites, leading to models that do not generalize well and cannot model complex local changes. We propose a new semi-supervised training strategy that addresses this problem and lets us learn complex local appearance harmonization from unpaired real composites, where foreground and background come from different images. Our model is fully parametric. It uses RGB curves to correct the global colors and tone and a shading map to model local variations. Our method outperforms previous work on established benchmarks and real composites, as shown in a user

study, and processes high-resolution images interactively.

1. Introduction

Image harmonization [12, 22, 23, 26, 28, 32] aims to iron out visual inconsistencies created when compositing a foreground subject onto a background image that was captured under different conditions [18, 32], by altering the foreground’s colors, tone, etc., to make the composite more realistic. Despite significant progress, the practicality of today’s most sophisticated learning-based image harmonization techniques [3, 4, 9, 10, 13, 14, 16, 32] is limited by a severe domain gap between the synthetic data they are trained on and real-world composites.

As shown in Figure 2, the standard approach to generating synthetic training composites applies global transforms (color, brightness, contrast, etc.) to a masked foreground subject in a ground truth photo. This is how the iHarmony

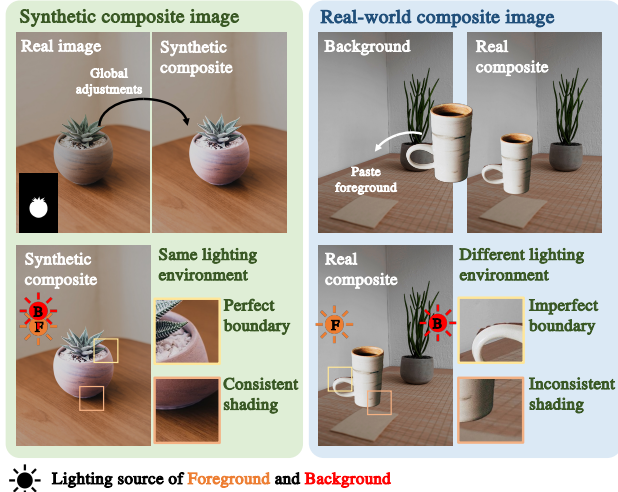


Figure 2. **Domain Gap between synthetic and real-world composites.** The existing synthetic composites [4] (left), generated by applying global transforms (e.g., color, brightness), are unable to simulate many of the appearance mismatches that occur in real composites (right). This leads to a domain gap: models trained on synthetic data do not generalize well to real composites. In real composites (right), the foreground and background are captured under different conditions. They have different illuminations, the shadows do not match, and the object’s boundary is inconsistent. Such mismatches do not happen in the synthetic case (left).

Dataset [2,4] was constructed. A harmonization network is then trained to recover the ground truth image from the synthetic input. While this approach makes supervised training possible, it is unsatisfying in simulating the real composite in that synthetic data does not simulate mismatch in illumination, shadows, shading, contacts, perspective, boundaries, and low-level image statistics like noise, lens blur, etc. However, in real-world composites, the foreground subject and the background are captured under different conditions, which can have more diverse and arbitrary differences in any aspects mentioned above.

We argue that using realistic composites for training is essential for image harmonization to generalize better to real-world use cases. Because collecting a large dataset of artist-created before/after real composite pairs would be costly and cumbersome, our strategy is to use a semi-supervised approach instead. We propose a novel dual-stream training scheme that alternates between two data streams. Similar to previous work, the first is a supervised training stream, but crucially, it uses artist-retouched image pairs. Different from previous datasets, these artistic adjustments include global color editing but also dodge and burn shading corrections and other local edits.

The second stream is fully unsupervised. It uses a GAN [8] training procedure, in which the critic compares our harmonized results with a large dataset of realistic image composites. Adversarial training requires no paired

ground truth. The foreground and background for the composite in this dataset are extracted from different images so that their appearance mismatch is consistent with what the model would see at test time.

To reap the most benefits from our semi-supervised training, we also introduce a new model that is fully parametric. To process a high-resolution input composite at test time, our proposed network first creates a down-sampled copy of the image at 512×512 resolution, from which it predicts *global RGB curves* and a smooth, low-resolution *shading map*. We then apply the RGB curves pointwise to the high-resolution input and multiply them by the upsampled shading map. The shading map enables more realistic local tonal variations, unlike previous harmonization methods limited to global tone and color changes, either by construction [14, 16, 31] or because of their training data [4].

Our parametric approach offers several benefits. First, by restricting the model’s output space, it regularizes the adversarial training. Unrestricted GAN generators often create spurious image artifacts or other unrealistic patterns [36]. Second, it exposes intuitive controls for an artist to adjust and customize the harmonization result post-hoc. This is unlike the black-box nature of most current learning-based approaches [3, 4, 9, 10], which output an image directly. And, third our parametric model runs at an interactive rate, even on very high-resolution images (e.g., 4k), whereas several state-of-the-art methods [4, 9, 10] are limited to low-resolution (e.g., 256×256) inputs.

To summarize, we make the following contributions:

- A novel dual-stream semi-supervised training strategy that, for the first time, enables training from real composites, which contains much richer local appearance mismatches between foreground and background.
- A parametric harmonization method that can capture these more complex, local effects (using our shading map) and produces more diverse and photorealistic harmonization results.
- State-of-the-art results on both synthetic and real composite test sets in terms of quantitative results and visual comparisons, together with a new evaluation benchmark.

We will release our code publicly upon publication.

2. Related works

Image harmonization. Traditional image harmonization methods mainly focus on adjusting the low-level appearance statistics (e.g., color statistics, gradient information) between the foreground objects and the background [12, 22, 23, 26, 28, 32]. Supervised learning-based approaches have been proposed and shown notable success [3, 4, 9, 10, 29, 37] by learning image harmonization from synthetic training pairs, for instance, iHarmony Dataset [4]. Works as DIH

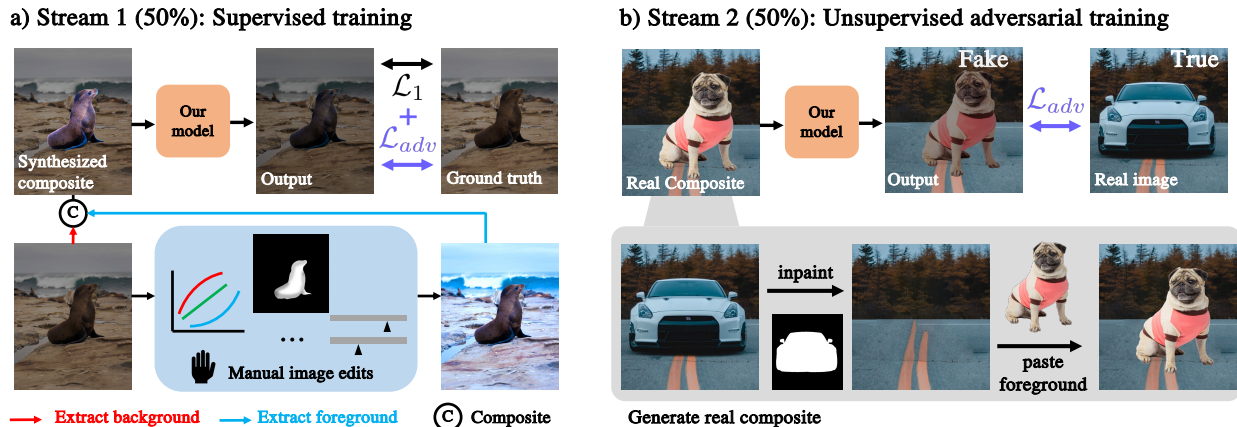


Figure 3. **Overview of semi-supervised dual-stream training strategy.** To bridge the domain gap, our proposed semi-supervised dual-stream training strategy alternates between two training streams: a) Supervised training with artist-retouched composite image pairs (left). Artist adjustments include global color editing, shading correction, and other local edits. b) Unsupervised adversarial training with real-world composite images (right). It uses a GAN [8] training procedure, comparing our harmonized results with a large dataset of realistic image composites. The foreground and background for the composite are from different images, so the appearance mismatch is consistent with what we see at test time.

[29], DovNet [4], IHT [9], Guo *et al.* [10] consider the image harmonization task as a pixel-wise image-to-image translation task, and are limited to low-resolution inputs (typically 256×256) due to computational inefficiency. Recent work extended image harmonization to high-resolution images by designing parametric models [3, 14, 16, 31]. To name a few, Liang *et al.* learns the spatial-separated RGB curves for high-resolution image harmonization. Ke *et al.* [14] directly predicts the filter arguments of several white-box filters, which can be efficiently applied to high-resolution images. In all of those approaches, synthetic training pairs are generated by applying global transforms to the masked foreground subjects of natural ground-truth images and hence do not simulate mismatch in illumination, shadows, shading, contact, etc., that happen in real-world composite images. Therefore, due to the synthetic training data and model construction [14, 16], previous works are limited to global tone and color changes. In contrast, our model is trained on real-world composite images and artist-retouched synthetic images, which enables us to model richer image edits and produce more compelling results on real composites.

Efficient and high-resolution image enhancement. There has been a wide range of research focusing on designing efficient and high-resolution image enhancement algorithms [6, 7, 17]. Gharbi *et al.* [6] introduced a convolutional neural network (CNN) that predicts the coefficients of a locally-affine model in bilateral space from down-sampled input images. The coefficients are then mapped back to the full-resolution image space. Zeng *et al.* [34] directly learns 3D Lookup Tables (LUTs) for real-time image enhancement. In our application, image harmonization can be considered as

a background-guided image enhancement problem. Thus, inspired by [6, 34], we design a network that directly predicts the coefficients of RGB curves (piece-wise linear function) from down-sampled composite inputs. We then apply the RGB curves pointwise to the high-resolution input without introducing extra computation costs.

Image-based relighting Image-based relighting approaches [19, 21, 25, 33] focus on modifying the input lighting conditions and local shading to generate convincing composite results. However, recent relighting methods are mainly designed for portrait applications and do not generalize well to other objects due to the limitation of Light-stage capturing only portraits but not diverse objects [5]. With a similar idea of incorporating local shading edits but a different approach, our method embeds the shading layer into a network and trains on composite image datasets without explicitly leveraging scene representations (geometry, materials, lighting) and using full relighting models.

3. Method

Our image harmonization method corrects the foreground subject in a rough composite to make the overall image look more realistic using a new parametric model (§ 3.1) that can be applied to real-world high-resolution images efficiently. Previous harmonization techniques train on synthetically-generated composite pairs [4], where the model’s input is a global transformation of a ground truth image within a foreground subject mask. The colors are often unnatural, the mask boundary is close to perfect, and there is no mismatch in appearance, illumination, or low-level image statistics since both foreground and background

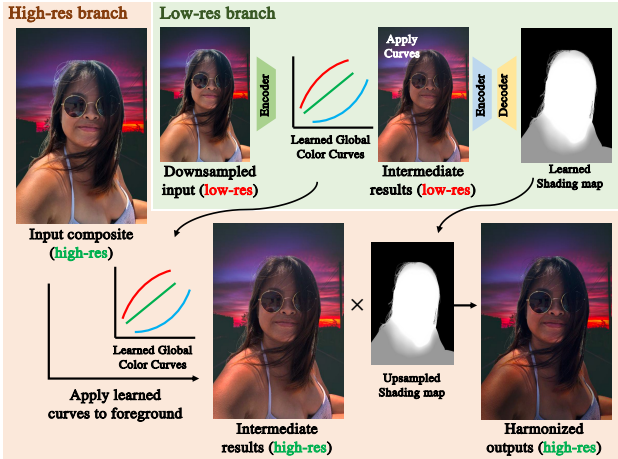


Figure 4. **Illustration of our parametric model design.** Our framework consists of a low-resolution branch and a high-resolution branch. At test time, we down-sample the given high-resolution image and predict the *global RGB curves and shading map* through a two-stage network. Those parametric outputs are then executed at the original resolution to produce the final harmonized image. Our model can scale to any resolution.

come from the same image. As a result, models trained on such data generalize poorly. Our method addresses this crucial issue using a novel dual-stream semi-supervised training strategy (§ 3.2) that leverages high-quality artist-created image pairs and unpaired realistic composites to bridge the training-testing domain gap. See Figure 3 for an overview.

3.1. Parametric image harmonization

Our network design is inspired by real-world composite harmonization workflows¹. An artist typically applies several image corrections sequentially, each dedicated to harmonizing a specific composite element, such as luminosity, color, or shading. Accordingly, our image transformation model consists of two modules, applied sequentially: a pointwise global color correction using RGB curves and a local shading correction using a low-frequency multiplicative map. For efficiency, our model operates at two resolutions.

Pipeline overview. As illustrated in Figure 4, our harmonization pipeline takes as input a foreground image $F \in \mathbb{R}^{3hw}$ with dimensions $h, w \in \mathbb{N}$, a background image image $B \in \mathbb{R}^{3hw}$, and a compositing alpha mask $M \in \mathbb{R}^{hw}$. We define the *unharmonized* composite image as $C := M \cdot F + (1 - M) \cdot B$. At test time, we start by downsampling the inputs to a fixed resolution (512×512), denoting the low-resolution images by C^{lr}, B^{lr}, M^{lr} respectively. We concatenate these maps and pass them to a neural network f that predicts the parameters $[\theta_1, \theta_2] := f(C^{lr}, B^{lr}, M^{lr})$

¹<https://youtu.be/g3qe4rDw1XU>

of our two-stage parametric image transformation. Finally, we apply the parametric transformation t_1, t_2 sequentially on the high-resolution input to obtain the final harmonized composite $O := t_2(t_1(C, M; \theta_1), M; \theta_2)$, where M is used to ensure only the area under the foreground mask is altered. We describe the two stages in the parametric transformation next.

Global color correction curves. Our first high-resolution processing stage t_1 applies the predicted global RGB curves for color correction. We parameterize them as 3 piecewise linear curves with 32 control points, applied to each color channel independently so that $\theta_1 \in \mathbb{R}^{32 \times 2 \times 3}$ is the set of 2D coordinates of the curve nodes. We predict these parameters from $[C^{lr}, B^{lr}, M^{lr}]$ using a ResNet-50 [11]-based network. Applying the curve is a per-pixel operation that can be efficiently computed at any resolution.

Local low-frequency shading map. Our second stage t_2 multiplies the image with a low-frequency grayscale shading map, to model local tonal corrections. It is applied on the output of the first stage. We constrain the shading map to only model low-frequency change by generating at a low resolution: $\theta_2 \in \mathbb{R}^{64 \times 64}$. It is produced by a modified U-Net [24] with large receptive field, given the low-resolution buffers $[C^{lr}, B^{lr}, M^{lr}]$, together with the output of the color-correction stage at low-resolution $t_1(C^{lr}, M^{lr}; \theta_1)$. At test time, we upsample the low-resolution shading map to the original high-resolution and multiply it pointwise with the color-corrected image to obtain our final harmonized composite:

$$O = t_1(C, M; \theta_1) \cdot \text{upsample}(\theta_2). \quad (1)$$

3.2. Dual-stream semi-supervised training

Our semi-supervised training strategy aims to alleviate the generalization issues that plague many state-of-the-art harmonization models, as shown in Figure 2. Our approach uses two data streams, sampled with equal probability, and minimizes a different objective on each data stream. The first stream uses input/output composite pairs similar to previous work, except that we only use artist-created image transformations instead of random augmentations. The second is unsupervised. This allows us to use more realistic images obtained by compositing foreground and background from unrelated images, for which no ground truth is easily obtainable. The objective for the supervised stream is the combination of ℓ_1 loss and adversarial loss, while we only impose adversarial loss for the unsupervised training stream.

Supervised training using retouched images. The first stream is fully supervised. Unlike previous work, we use images retouched by artists rather than mostly relying on random augmentations. We refer to this dataset as *Artist-Retouched* in the rest of the paper. Artists were allowed

to use common image editing operations such as global luminosity or color adjustments, but also local editing tools like brushes, e.g., to alter the shading. Specifically, we collected $n = 46173$ before/after retouching image pairs $\{\mathbf{I}_i, \mathbf{O}_i\}_{i=1, \dots, n}$, with the mask for one foreground object \mathbf{M}_i for each pair. From each triplet, we can create 2 input composites for training: one with only the foreground retouched $\mathbf{M}_i \cdot \mathbf{O}_i + (1 - \mathbf{M}_i) \cdot \mathbf{I}_i$, and the other with only the background is retouched $\mathbf{M}_i \cdot \mathbf{I}_i + (1 - \mathbf{M}_i) \cdot \mathbf{O}_i$. Since our harmonization model only alters the foreground, we use the unedited image \mathbf{I}_i , and the retouched image \mathbf{O}_i as ground truth targets for these input composites, respectively.

When sampling training data from this stream, we optimize our model’s parameters to minimize the sum of an ℓ_1 reconstruction error \mathcal{L}_{rec} between the ground truth and our model output, and an adversarial objective [8]

$$\lambda \mathcal{L}_{rec} + (1 - \lambda) \mathcal{L}_G, \quad (2)$$

with λ balances the two losses. For our experiments, λ is empirically set to 0.92. The generator, our parametric image harmonization model, is trained to produce outputs that cannot be distinguished from “real” images. We use a U-Net discriminator [30] D to make per-pixel real vs. fake classifications. Since our data formation model assumes the background is always correct, our discriminator is trained to predict the inverted foreground mask $1 - \mathbf{M}$. That is when shown “fake” images, i.e., the background pixels have label 1 and the foreground 0. For the “real” class, the target is all an all-1s map. So the discriminator loss is given by:

$$\begin{aligned} \mathcal{L}_D = & -\mathbb{E}_{\mathbf{I}_{real}} [\log(D(\mathbf{I}_{real}))] \\ & -\mathbb{E}_{\mathbf{I}_{fake}} [\log((1 - \mathbf{M}) - D(\mathbf{I}_{fake}))], \end{aligned} \quad (3)$$

The generator loss is:

$$\mathcal{L}_G = -\mathbb{E}_{\mathbf{I}_{fake}} [\log(D(\mathbf{I}_{fake}))]. \quad (4)$$

To further increase the training diversity, we randomly augment the foreground brightness on the fly without retouching the color.

Unsupervised training with real composites. Our second training stream is unsupervised. It uses randomly generated composites that are representative of real-world use cases but for which no ground truth is available. To properly reproduce the appearance mismatch in real applications, we create these composites as follows. We start from a dataset of m images $\{\mathbf{I}_i\}_{i=1, \dots, m}$, each with a foreground object mask \mathbf{M}_i , from which we derive a foreground $\mathbf{F}_i = \mathbf{M}_i \cdot \mathbf{I}_i$ and a background $\mathbf{B}_i = (1 - \mathbf{M}_i) \cdot \mathbf{I}_i$. As preprocessing, we dilate the foreground mask by 30 pixels and inpaint the corresponding area in the background image using a pre-trained inpainting network (we use LaMa [27]). Then during training we sample two images i and j and create a composite by pasting the foreground j onto the inpainted background of i :

$$\mathbf{C}_{ij} := \mathbf{F}_j \cdot \mathbf{M}_j + \text{inpaint}(\mathbf{B}_i, \mathbf{M}_i) \cdot (1 - \mathbf{M}_j). \quad (5)$$

The triplet $[\mathbf{C}_{ij}, \text{inpaint}(\mathbf{B}_i, \mathbf{M}_i), \mathbf{M}_j]$ is passed as input to our model. Figure 3b illustrates the process.

With no ground truth available when sampling composites from this data stream, we only optimize the adversarial loss $(1 - \lambda) \mathcal{L}_G$, as defined in Eq. (4), where again the fake samples \mathbf{I}_{fake} are the outputs of our model.

The discriminator is trained with Eq. (3), where \mathbf{I}_{real} is not a real composite, but is obtained by masking the foreground subject \mathbf{F}_i , inpainting the background \mathbf{B}_i , and pasting the foreground back onto the same image, i.e.

$$\mathbf{I}_{real} := \mathbf{F}_i \cdot \mathbf{M}_i + \text{inpaint}(\mathbf{B}_i, \mathbf{M}_i) \cdot (1 - \mathbf{M}_i). \quad (6)$$

This is similar to how we produce a composite of two images i and j , except that we only use one image, i . This alteration of the “real” class is to prevent the discriminator from using the inpainting boundary region as a strong cue to discriminate between our model output and real images, which leads to collapse in the GAN training.

GAN training is known to be unstable or cause image artifacts [36], but because our parametric harmonization model adjusts color curves and adds low-resolution shadows, instead of predicting pixels directly, it has a strong regularizing effect, which prevents the GAN training to degenerate and cause spurious artifacts in the output image. We use the same discriminator (and generator) in both streams.

4. Experiments

We compare our parametric image harmonization model with state-of-the-art methods on several established benchmarks (§ 4.1), as well as a test subset of *Artist-Retouched* dataset. Furthermore, we demonstrate our superior performance on real-world harmonization tasks via a user study and qualitative comparisons on real composites (§ 4.2). Ablations of our method demonstrate the benefits of our semi-supervised training strategy and the individual components of our parametric model (§ 4.3). More results can be found in the supplementary.

Evaluation metrics: For quantitative comparisons with ground truth, we report performances by Mean Square Error (MSE), Peak Signal-to-Noise Ratio (PSNR), Structural Similarity (SSIM), and Learned Perceptual Image Patch Similarity (LPIPS) [35]. PSNR is measured in dB and calculated as: $\text{PSNR} = 10 \log_{10} \frac{255^2}{\text{MSE}}$.

Implementation details: Our model and discriminator are implemented in PyTorch [20] and trained on an NVIDIA A100 GPU using the Adam optimizer [15] for 80 epochs, with a batch size of 8 and an initial learning rate of 4×10^{-5} , decayed by a factor 0.2 every 20 epochs.

4.1. Quantitative comparisons on paired data

We compare our method with three recent methods, DovNet [4], Image Harmonization with Transformer



Figure 5. **Representative visual comparisons between state-of-the-art harmonization results.** We compared our method with composite, DovNet [4], IHT [9], and Harmonizer [14], and ground truth on both a) *Artist-Retouched* synthetic dataset and b) RealHM real-world composite dataset. Red boxes indicate the foreground subject in the composite image. The ground truth for RealHM benchmark [13] is expert-annotated harmonization results. Our results show better visual agreements with the ground truth in terms of color harmonization (rows 1,2 and 4) and shading correction (row 3).

(IHT) [14], and Harmonizer [14], using the pre-trained model released publicly by the authors. We first evaluate the synthetic iHarmony benchmark [4]. For fairness, our method uses the same setup as theirs for this comparison. In particular, we train our model exclusively on the same training set as the baselines, using only our fully-supervised stream, deactivating the adversarial loss, and only passing the composite C and foreground mask M as inputs. We report metrics at both at 256×256 resolution and at 2048×2048 on the HAdobe5k high-resolution subset of iHarmony. Like our parametric approach, Harmonizer can process high-res images, but the other two methods are limited to 256×256 inputs. So, for high-res comparison, we bilinearly downsample the input to DovNet and IHT, process the image, then bilinearly upsample the result before computing the metrics. Despite its simplicity, our parametric model consistently outperforms or matches the more complex baselines. Results are summarized in Table 1.

The iHarmony dataset is dominated by unrealistic synthetic image augmentations (71%), so we also evaluate our results on more realistic retouches from human experts. The two datasets we use for evaluation are a testing split of our *Artist-Retouched* dataset, introduced in Section 3.2, containing 1000 before/after pairs, and the RealHM [13] benchmark, containing 216 real-world high-resolution composites with expert annotated harmonization results as ground

Size	Method	MSE ↓	PSNR ↑	SSIM ↑ $\times 10^{-2}$	LPIPS ↓ $\times 10^{-3}$
256	Composite	172.3	31.74	97.48	16.46
	DovNet [4]	51.33	34.97	98.12	9.734
	IHT [9]	30.46	37.33	98.77	7.347
	Harmonizer [14]	24.24	38.25	99.09	7.349
	Ours	20.57	38.30	98.91	7.270
2048*	Composite	352.9	28.39	96.36	14.52
	DovNet [4]	66.37	34.01	96.35	21.45
	IHT [9]	47.34	35.12	96.53	20.65
	Harmonizer [14]	23.30	38.33	98.77	7.148
	Ours	20.31	38.29	98.82	7.123

Table 1. **Quantitative comparison on iHarmony benchmark [4]** at both 256×256 and 2048×2048 . (*) We only calculate the metrics on the Adobe5k dataset (a subset of iHarmony4) for high-resolution images. **Red**, and **Blue** correspond to the first and second best results. \uparrow means higher the better, and \downarrow means lower the better.

truth. We compared the performance of their pre-trained models and ours trained with the full dual-stream pipeline at 2048×2048 resolution. Table 2 shows our method consistently outperforms the baselines, with around 30% relative MSE improvements compared to Harmonizer [14] on both datasets. As shown in Figure 5, our method produces more

Dataset	Method	MSE ↓	PSNR ↑	SSIM ↑ $\times 10^{-2}$	LPIPS ↓ $\times 10^{-3}$
Artist-Retouched	Composite	603.20	23.41	91.19	40.18
	DovNet [4]	352.4	26.42	90.83	56.47
	IHT [9]	369.3	26.36	90.87	55.80
	Harmonizer [14]	239.1	29.42	93.84	33.75
	Ours	170.1	29.79	94.56	29.18
RealHM	Composite	404.4	25.88	94.70	29.32
	DovNet [4]	225.1	26.72	92.00	47.50
	IHT [9]	264.0	26.48	92.46	48.48
	Harmonizer [14]	231.4	27.40	94.86	27.62
	Ours	153.3	28.34	95.51	23.09

Table 2. **Quantitative Comparison on RealHM benchmark and Artist-Retouched dataset.** Our approach outperforms other methods in all four metrics.

realistic results, closer to the ground truth.

4.2. Evaluation on real composite images

Our semi-supervised training procedure allows us to train on realistic composites, where foreground and background come from different sources. Just like it limits the training potential of harmonization methods, using paired data created from a single ground truth image for evaluation is unsatisfying because it is not representative of real-world use cases (Fig. 2). So, we demonstrate the practical effectiveness of our method in a user study with real composites. For qualitative evaluation, we also created a set of 40 high-resolution real composite images with reference images.

User Study. Our user study follows a 2 alternatives forced choice protocol [35], comparing our model with DovNet [4], IHT [9], and Harmonizer [14]. We selected 60 real composites from the RealHM dataset [13], making sure there were no duplicate foregrounds or backgrounds. Since RealHM primarily focuses on portrait images, we also created 40 non-portrait real composites using free-to-use images from Unsplash², giving us a total of 100 real composite images. Each of our results is compared with the unaltered input composite and the three baseline results, which gives $100 \times 4 = 400$ image pairs to compare in total, which we submitted for evaluation to a pool of subjects on Amazon Turk³. Each participant was shown 50 image pairs and, for each pair, they were asked to “select which image looks more plausible”. To ensure the quality of the responses, each subject was also shown 10 ‘sentinel’ testing pairs composed of a real natural image and an extremely off-retouch image (e.g., where the image is all green). This helped us filter low-quality participants, such as users that always click ‘left’ to try and game the MTurk reward. After filtering, we obtained pair-wise comparison results from

²<https://unsplash.com/>

³<https://www.mturk.com/>

70 subjects, contributing a total of 3500 comparisons. To analyze these results, we follow previous work [3, 4, 14], and use the Bradley-Terry (B-T) [1] model to derive the global ranking of all methods. We normalize the B-T scores such that the sum of the scores equals one across methods. Table 3 summarizes the results. It shows that our method achieves the highest B-T score, outperforming all the baselines, indicating our approach compares favorably in real-world applications.

Methods	B-T Score ↑
Composite	0.1025
DovNet [4]	0.1342
IHT [9]	0.2350
Harmonizer [14]	0.2257
Ours	0.3025

Table 3. **User Study Results.** B-T scores of composite image, DovNet [4], IHT [9], Harmonizer [14] are calculated on 100 real composite images. Our approach ranks first, suggesting superior real-world performance.

Real composites with captured reference. Figure 6 shows two representative examples of real composite results (see supplemental for more). For this qualitative comparison, we created a dataset of 40 high-resolution real-composite images with reference images by capturing a fixed set of foreground objects against multiple backgrounds, as well as a ‘background-only’ image. By segmenting the foreground object from one photo and pasting onto the ‘background-only’ image of another, we get an input composite for our model. The captured photo of the same object in the same background scene (placed at roughly the same location) acts as qualitative reference. Compared to other approaches, our results are visually closer to the captured reference.

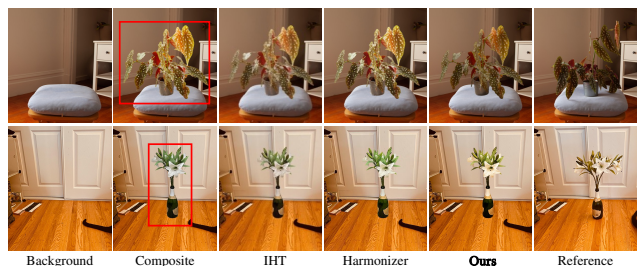


Figure 6. **Real composite harmonization results with captured reference.** The composite is obtained by pasting the foreground subject, from a different photo (not shown) onto the background (left). The reference (right) is obtained by physically placing the foreground subject in the background scene and taking a photo. We compare our method with IHT [9], and Harmonizer [14]. Our results show better visual agreement with the captured reference (best viewed by zooming on the digital preprint).

4.3. Ablation studies

We evaluate the benefits of our dual-stream semi-supervised training strategy, comparing it to conventional supervised training. We also analyze the impact of our global RGB curve module and shading map. We conduct the comparisons on RealHM [13] at 512×512 resolution, comparing our full method (dual-stream training + two-stage model) with: 1. Supervised training only (Stream 1) + global curves only; 2. Supervised training only (Stream 1) + two-stage parametric model; 3. Dual-stream training + global curves module only. We report quantitative metrics (MSE and PSNR), and the B-T score from a user study (similar to § 4.2, but this time with 68 subjects) Table 4 and Figure 7 summarize our results. They show our shading map and our dual-stream training strategy both significantly improve realism over the curve-only, fully-supervised model.

Stream 1	Stream 2	Global Curves	Shading Map	MSE	PSNR	B-T score
✓		✓		288.7	26.45	0.201
✓		✓	✓	264.0	26.89	0.206
✓	✓	✓		222.6	27.29	0.217
✓	✓	✓	✓	154.3	28.40	0.252
Composite				-	-	0.124

Table 4. **Ablation study results of training strategies and parametric model.** We compare our semi-supervised training strategy (Stream 1 + Stream 2) with supervised training (Stream 1) and compare our two-stage model (Global Curves + Shading map) versus the model with only the global curve module. MSE and PSNR are used for quantitative comparisons, and the B-T score is calculated from user study results.

As reported in Table 4, we observe that the dual-stream training strategy outperforms supervised training (row 3 and 4 v.s. row 1 and 2) in terms of both quantitative metrics and B-T score, which demonstrates the benefits of our proposed dual-training strategy in real-world applications. Inspecting the results in Figure 7, we observe that the dual-training strategy (column 4 and 5) brings advantages in color-harmonization when there is a strong foreground-background color mismatch.

On the other hand, as shown in Table 4 row 3 v.s. row 4, our proposed two-stage parametric model outperforms the global curve-only model by a large margin on RealHM benchmark, reducing the MSE by 30%. Furthermore, as shown in Figure 7, our full model (last column) includes both color harmonization and local shading to the results, achieving more plausible and harmonious results.

To better visualize the roles of our two-stage parametric model, Figure 8 shows the intermediate results as well as the parametric outputs (global curves and shading map) of

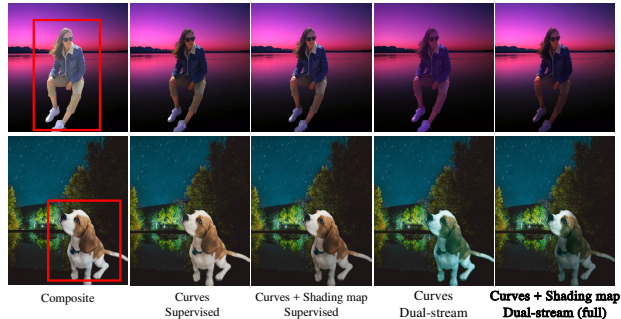


Figure 7. **Visual comparison of ablations.** Our full pipeline (right) shows more color-harmonious results than supervised training-only models (columns 2 and 3). Our local shading map adjusts local shading and produces more natural outputs (compare columns 4 and 5).

a representative example. The global curves module harmonizes the global tone of the foreground sculpture and matches it with the background scene. The shading map module further performs local editing to adjust the shading of the sculpture and fit it with the lighting environment better.

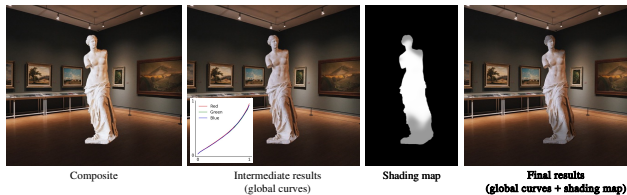


Figure 8. **Intermediate results and parametric outputs.** RGB curves harmonize the global color/tone (center), while our shading map corrects the local shading in the harmonization output (right).

5. Conclusion

In this work, we propose a novel semi-supervised dual-stream training strategy to bridge the training-testing domain gap and mitigate the generalization issues that limit previous works for real-world image harmonization. Our method leverages high-quality artist-created image pairs and unpaired realistic composites to enable richer image edits for real-world applications. Besides, we introduce a new two-stage parametric model (*Global RGB Curves* and *shading map*) to reap the most benefits from our training strategy and, for the first time, enable local editing effects with learned shading map. Our method outperforms other state-of-the-art methods on established benchmarks and real composites. Furthermore, our training strategy has the potential to generalize to a wider range of image harmonization operations (e.g., matching the noise, harmonizing the boundaries, adding cast shadows). As a future work, we would like to include more attributes in our models and further improve the performance of real-world image harmonization.

References

- [1] Ralph Allan Bradley and Milton E Terry. Rank analysis of incomplete block designs: I. the method of paired comparisons. *Biometrika*, 39(3/4):324–345, 1952. [7](#)
- [2] Vladimir Bychkovsky, Sylvain Paris, Eric Chan, and Frédo Durand. Learning photographic global tonal adjustment with a database of input / output image pairs. In *The Twenty-Fourth IEEE Conference on Computer Vision and Pattern Recognition*, 2011. [2](#)
- [3] Wenyan Cong, Xinhao Tao, Li Niu, Jing Liang, Xuesong Gao, Qihao Sun, and Liqing Zhang. High-resolution image harmonization via collaborative dual transformations. In *Proceedings of the IEEE/CVF Conference on Computer Vision and Pattern Recognition*, pages 18470–18479, 2022. [1](#), [2](#), [3](#), [7](#)
- [4] Wenyan Cong, Jianfu Zhang, Li Niu, Liu Liu, Zhixin Ling, Weiyan Li, and Liqing Zhang. Dovenet: Deep image harmonization via domain verification. In *Proceedings of the IEEE/CVF Conference on Computer Vision and Pattern Recognition*, pages 8394–8403, 2020. [1](#), [2](#), [3](#), [5](#), [6](#), [7](#), [11](#), [12](#), [13](#), [14](#), [15](#), [16](#), [17](#), [18](#)
- [5] Paul Debevec, Tim Hawkins, Chris Tchou, Haarm-Pieter Duiker, Westley Sarokin, and Mark Sagar. Acquiring the reflectance field of a human face. In *Proceedings of the 27th annual conference on Computer graphics and interactive techniques*, pages 145–156, 2000. [3](#)
- [6] Michaël Gharbi, Jiawen Chen, Jonathan T Barron, Samuel W Hasinoff, and Frédo Durand. Deep bilateral learning for real-time image enhancement. *ACM Transactions on Graphics (TOG)*, 36(4):1–12, 2017. [3](#)
- [7] Michaël Gharbi, YiChang Shih, Gaurav Chaurasia, Jonathan Ragan-Kelley, Sylvain Paris, and Frédo Durand. Transform recipes for efficient cloud photo enhancement. *ACM Transactions on Graphics (TOG)*, 34(6):1–12, 2015. [3](#)
- [8] Ian Goodfellow, Jean Pouget-Abadie, Mehdi Mirza, Bing Xu, David Warde-Farley, Sherjil Ozair, Aaron Courville, and Yoshua Bengio. Generative adversarial networks. *Communications of the ACM*, 63(11):139–144, 2020. [2](#), [3](#), [5](#)
- [9] Zonghui Guo, Dongsheng Guo, Haiyong Zheng, Zhaorui Gu, Bing Zheng, and Junyu Dong. Image harmonization with transformer. In *Proceedings of the IEEE/CVF International Conference on Computer Vision*, pages 14870–14879, 2021. [1](#), [2](#), [3](#), [6](#), [7](#), [11](#), [12](#), [13](#), [14](#), [15](#), [16](#), [17](#), [18](#)
- [10] Zonghui Guo, Haiyong Zheng, Yufeng Jiang, Zhaorui Gu, and Bing Zheng. Intrinsic image harmonization. In *Proceedings of the IEEE/CVF Conference on Computer Vision and Pattern Recognition*, pages 16367–16376, 2021. [1](#), [2](#), [3](#)
- [11] Kaiming He, Xiangyu Zhang, Shaoqing Ren, and Jian Sun. Deep residual learning for image recognition. In *Proceedings of the IEEE conference on computer vision and pattern recognition*, pages 770–778, 2016. [4](#)
- [12] Jiaya Jia, Jian Sun, Chi-Keung Tang, and Heung-Yeung Shum. Drag-and-drop pasting. *ACM Transactions on Graphics (TOG)*, 25(3):631–637, 2006. [1](#), [2](#)
- [13] Yifan Jiang, He Zhang, Jianming Zhang, Yilin Wang, Zhe Lin, Kalyan Sunkavalli, Simon Chen, Sohrab Amirghodsi, Sarah Kong, and Zhangyang Wang. Ssh: A self-supervised framework for image harmonization. In *Proceedings of the IEEE/CVF International Conference on Computer Vision*, pages 4832–4841, 2021. [1](#), [6](#), [7](#), [8](#), [11](#), [12](#)
- [14] Zhanghan Ke, Chunyi Sun, Lei Zhu, Ke Xu, and Rynson WH Lau. Harmonizer: Learning to perform white-box image and video harmonization. *arXiv preprint arXiv:2207.01322*, 2022. [1](#), [2](#), [3](#), [6](#), [7](#), [11](#), [12](#), [13](#), [14](#), [15](#), [16](#), [17](#), [18](#)
- [15] Diederik P Kingma and Jimmy Ba. Adam: A method for stochastic optimization. *arXiv preprint arXiv:1412.6980*, 2014. [5](#)
- [16] Jingtang Liang, Xiaodong Cun, and Chi-Man Pun. Spatial-separated curve rendering network for efficient and high-resolution image harmonization. *arXiv preprint arXiv:2109.05750*, 2021. [1](#), [2](#), [3](#)
- [17] Sean Moran, Pierre Marza, Steven McDonagh, Sarah Parisot, and Gregory Slabaugh. Deeplpf: Deep local parametric filters for image enhancement. In *Proceedings of the IEEE/CVF conference on computer vision and pattern recognition*, pages 12826–12835, 2020. [3](#)
- [18] Li Niu, Wenyan Cong, Liu Liu, Yan Hong, Bo Zhang, Jing Liang, and Liqing Zhang. Making images real again: A comprehensive survey on deep image composition. *arXiv preprint arXiv:2106.14490*, 2021. [1](#)
- [19] Rohit Pandey, Sergio Orts Escolano, Chloe Legendre, Christian Haene, Sofien Bouaziz, Christoph Rhemann, Paul Debevec, and Sean Fanello. Total relighting: learning to relight portraits for background replacement. *ACM Transactions on Graphics (TOG)*, 40(4):1–21, 2021. [3](#)
- [20] Adam Paszke, Sam Gross, Francisco Massa, Adam Lerer, James Bradbury, Gregory Chanan, Trevor Killeen, Zeming Lin, Natalia Gimelshein, Luca Antiga, et al. Pytorch: An imperative style, high-performance deep learning library. *Advances in neural information processing systems*, 32, 2019. [5](#)
- [21] Julien Philip, Sébastien Mordant, Michaël Gharbi, and George Drettakis. Free-viewpoint indoor neural relighting from multi-view stereo. *ACM Transactions on Graphics (TOG)*, 40(5):1–18, 2021. [3](#)
- [22] Francois Pitie, Anil C Kokaram, and Rozenn Dahyot. N-dimensional probability density function transfer and its application to color transfer. In *Tenth IEEE International Conference on Computer Vision (ICCV'05) Volume 1*, volume 2, pages 1434–1439. IEEE, 2005. [1](#), [2](#)
- [23] Erik Reinhard, Michael Adhikhmin, Bruce Gooch, and Peter Shirley. Color transfer between images. *IEEE Computer graphics and applications*, 21(5):34–41, 2001. [1](#), [2](#)
- [24] Olaf Ronneberger, Philipp Fischer, and Thomas Brox. U-net: Convolutional networks for biomedical image segmentation. In *International Conference on Medical image computing and computer-assisted intervention*, pages 234–241. Springer, 2015. [4](#)
- [25] Tiancheng Sun, Jonathan T Barron, Yun-Ta Tsai, Zexiang Xu, Xueming Yu, Graham Fyffe, Christoph Rhemann, Jay Busch, Paul E Debevec, and Ravi Ramamoorthi. Single image portrait relighting. *ACM Trans. Graph.*, 38(4):79–1, 2019. [3](#)
- [26] Kalyan Sunkavalli, Micah K Johnson, Wojciech Matusik, and Hanspeter Pfister. Multi-scale image harmonization.

- ACM Transactions on Graphics (TOG)*, 29(4):1–10, 2010. 1, 2
- [27] Roman Suvorov, Elizaveta Logacheva, Anton Mashikhin, Anastasia Remizova, Arsenii Ashukha, Aleksei Silvestrov, Naejin Kong, Harshith Goka, Kiwoong Park, and Victor Lempitsky. Resolution-robust large mask inpainting with fourier convolutions. In *Proceedings of the IEEE/CVF Winter Conference on Applications of Computer Vision*, pages 2149–2159, 2022. 5
- [28] Michael W Tao, Micah K Johnson, and Sylvain Paris. Error-tolerant image compositing. In *European Conference on Computer Vision*, pages 31–44. Springer, 2010. 1, 2
- [29] Yi-Hsuan Tsai, Xiaohui Shen, Zhe Lin, Kalyan Sunkavalli, Xin Lu, and Ming-Hsuan Yang. Deep image harmonization. In *Proceedings of the IEEE Conference on Computer Vision and Pattern Recognition*, pages 3789–3797, 2017. 2, 3
- [30] Xintao Wang, Liangbin Xie, Chao Dong, and Ying Shan. Real-esrgan: Training real-world blind super-resolution with pure synthetic data. In *Proceedings of the IEEE/CVF International Conference on Computer Vision*, pages 1905–1914, 2021. 5
- [31] Ben Xue, Shenghui Ran, Quan Chen, Rongfei Jia, Binqiang Zhao, and Xing Tang. Dccf: Deep comprehensible color filter learning framework for high-resolution image harmonization. *arXiv preprint arXiv:2207.04788*, 2022. 2, 3
- [32] Su Xue, Aseem Agarwala, Julie Dorsey, and Holly Rushmeier. Understanding and improving the realism of image composites. *ACM Transactions on graphics (TOG)*, 31(4):1–10, 2012. 1, 2
- [33] Yu-Ying Yeh, Koki Nagano, Sameh Khamis, Jan Kautz, Ming-Yu Liu, and Ting-Chun Wang. Learning to relight portrait images via a virtual light stage and synthetic-to-real adaptation. *ACM Transactions on Graphics (TOG)*, 2022. 3
- [34] Hui Zeng, Jianrui Cai, Lida Li, Zisheng Cao, and Lei Zhang. Learning image-adaptive 3d lookup tables for high performance photo enhancement in real-time. *IEEE Transactions on Pattern Analysis and Machine Intelligence*, 2020. 3
- [35] Richard Zhang, Phillip Isola, Alexei A Efros, Eli Shechtman, and Oliver Wang. The unreasonable effectiveness of deep features as a perceptual metric. In *Proceedings of the IEEE conference on computer vision and pattern recognition*, pages 586–595, 2018. 5, 7
- [36] Xu Zhang, Svebor Karaman, and Shih-Fu Chang. Detecting and simulating artifacts in gan fake images. In *2019 IEEE international workshop on information forensics and security (WIFS)*, pages 1–6. IEEE, 2019. 2, 5
- [37] Jun-Yan Zhu, Philipp Krahenbuhl, Eli Shechtman, and Alexei A Efros. Learning a discriminative model for the perception of realism in composite images. In *Proceedings of the IEEE International Conference on Computer Vision*, pages 3943–3951, 2015. 2

6. Supplementary material

In this supplementary, we first describe how our *Artist-Retouched* dataset was constructed, and show representative visual examples from the dataset (introduced in § 3.2). Then, we show the visual comparisons on iHarmony dataset [4] and report the detailed quantitative comparison results on four subsets (HCOCO, HAdobe5k, HFlickr, Hday2night). Besides, we provide more high-resolution visual results of different methods on the *Artist-Retouched* dataset and RealHM benchmark (supplementary to § 4.1). We then go in-depth into our real composite dataset with captured references and present more qualitative visual comparisons (supplementary to § 4.2). Furthermore, we show more visual comparisons of real composite images we used as part of our user studies (§ 4.2). Finally, we show more intermediate results and parametric outputs of our method for real-composite image harmonization (supplementary to § 4.3).

6.1. Artist-Retouched dataset

In this work, we propose to use a new *Artist-Retouched* dataset for our dual-stream training experiments. Unlike previous work, *Artist-Retouched* contains image pairs retouched by artists rather than mostly relying on random color augmentations. Artists were allowed to use global luminosity or color adjustments operations, but also local editing tools like brushes, e.g., to alter the shading. All the image editing was done using Adobe Lightroom, a software dedicated to photo adjustment. Figure S1 shows representative before-after image pairs in the *Artist-Retouched* dataset. *Artist-Retouched* consists of $n = 46173$ before/after retouching image pairs $\{\mathbf{I}_i, \mathbf{O}_i\}_{i=1,\dots,n}$, with the foreground mask \mathbf{M}_i for each pair. As visualized in the figure, the retouching procedure consists of global luminosity/color adjustments (e.g., exposure, contrast, Highlights, Temp, Tint, Hue) and local editing tools (e.g., adding shading, creating soft transitions by gradient mask). From each triplet $\{\mathbf{I}_i, \mathbf{O}_i, \mathbf{M}_i\}$, we can generate two synthetic composite inputs for training: one with only the foreground retouched $\mathbf{M}_i \cdot \mathbf{O}_i + (1 - \mathbf{M}_i) \cdot \mathbf{I}_i$, and the other one with only the background being retouched $\mathbf{M}_i \cdot \mathbf{I}_i + (1 - \mathbf{M}_i) \cdot \mathbf{O}_i$. We use the unedited image \mathbf{I}_i and the retouched image \mathbf{O}_i as ground truth targets of these composite inputs, respectively.

6.2. More results on iHarmony benchmark

As discussed in § 4.1, we evaluate our method on the iHarmony benchmark [4] and present the quantitative results on the entire dataset. In this section, we report the quantitative results on four subsets of iHarmony — HCOCO, HAdobe5k, HFlickr, Hday2night. We compare our method with DovNet [4], IHT [9], Harmonizer [14]. Our method outperforms or matches state-of-the-art approaches in all four subsets of iHarmony benchmark. Ta-

ble S1 summarizes the quantitative results. Besides, Figure S2 shows a gallery of selective visual comparisons between different approaches at 512×512 resolution. For better visualization, we resize the images to their original aspect ratios.

6.3. More visual results on Artist-retouched dataset

As introduced in § 3.2, we evaluate different methods on a testing split of our *Artist-Retouched* dataset with realistic retouches from human experts. In addition to the results shown in Figure 5, Figure S3 presents more visual comparisons on *Artist-Retouched* testing dataset at 1024 resolution. We observe that our results agree better with the ground truth images in terms of the visual quality compared to other methods (DovNet [4], IHT [9], Harmonizer [14]). Besides, we also show one failure example (boat), where all methods (including ours) fail to retrieve the correct color of the ground truth image, though some of them look harmonious by themselves without seeing the reference. We hypothesize that, in this case, the skylight illumination in the ground-truth image is difficult to infer from the background.

6.4. More visual results on RealHM benchmark

Different from synthetic dataset [4], RealHM [13] benchmark contains 216 real-world high-resolution composites with expert annotated harmonization results as ground truth. In this section, we present more visual harmonization comparisons in Figure S4 at 1024 resolution. From the results, we observe that even though there exist strong foreground/background color mismatches in the real composite images, our method produces more harmonious results compared to other approaches.

6.5. Real composites with captured reference

As briefly introduced in § 4.2, for qualitative evaluation, we created a dataset of 40 high-resolution real-composite images with captured references. As illustrated in Figure S5, we first capture a fixed set of foreground objects against multiple backgrounds (scenes), as well as the corresponding "background-only" images. We then segment the foreground object of one photo and paste it onto the "background-only" photo of another with roughly the same location. The captured photo of the same object in the same background scene serves as a reference for qualitative evaluation. Figure S6 visualize selective examples of the harmonization results. We compare our method with state-of-the-art approaches. As shown in the figure, for the first example, our result shows better visual agreements with the captured reference. For the second and third examples, though our results don't exactly match the reference (none of the other methods does), our method still produces images with harmonious appearances. We will release this

dataset upon publication.

6.6. More results on real composite images

Figure S7 shows more visual comparisons on real composite images where we don't have the ground truth or captured reference. We use these images as part of our user studies (§4.2). We compare our method with DovNet [4], IHT [9], Harmonizer [14]. We will release these testing real composite images upon the publication of this work.

6.7. More intermediate results

Figure S8 presents more intermediate results and parametric outputs on RealHM [13] real-composite benchmark. As shown in the results, our predicted RGB curves harmonize the global color/tone, while our learned shading map incorporates local shading to the final outputs. By comparing with the human-annotated harmonization results (right), we observe that our local shading maps align well with the local operation done by the human experts. For instance, for the top three rows, both our results and the human-annotated ground truth selectively darkened the bottom part of the foreground objects. For the fourth row example, our result highlights the region with incoming light while darkening other foreground parts, which agrees with the operations done by human experts.

6.8. Demo video

To further better demonstrate the effectiveness of our method in real-world applications, we prepared and recorded a demo video (see attachments of the supplementary material). We can interactively run our demo on a single CPU without access to extensive computing resources.

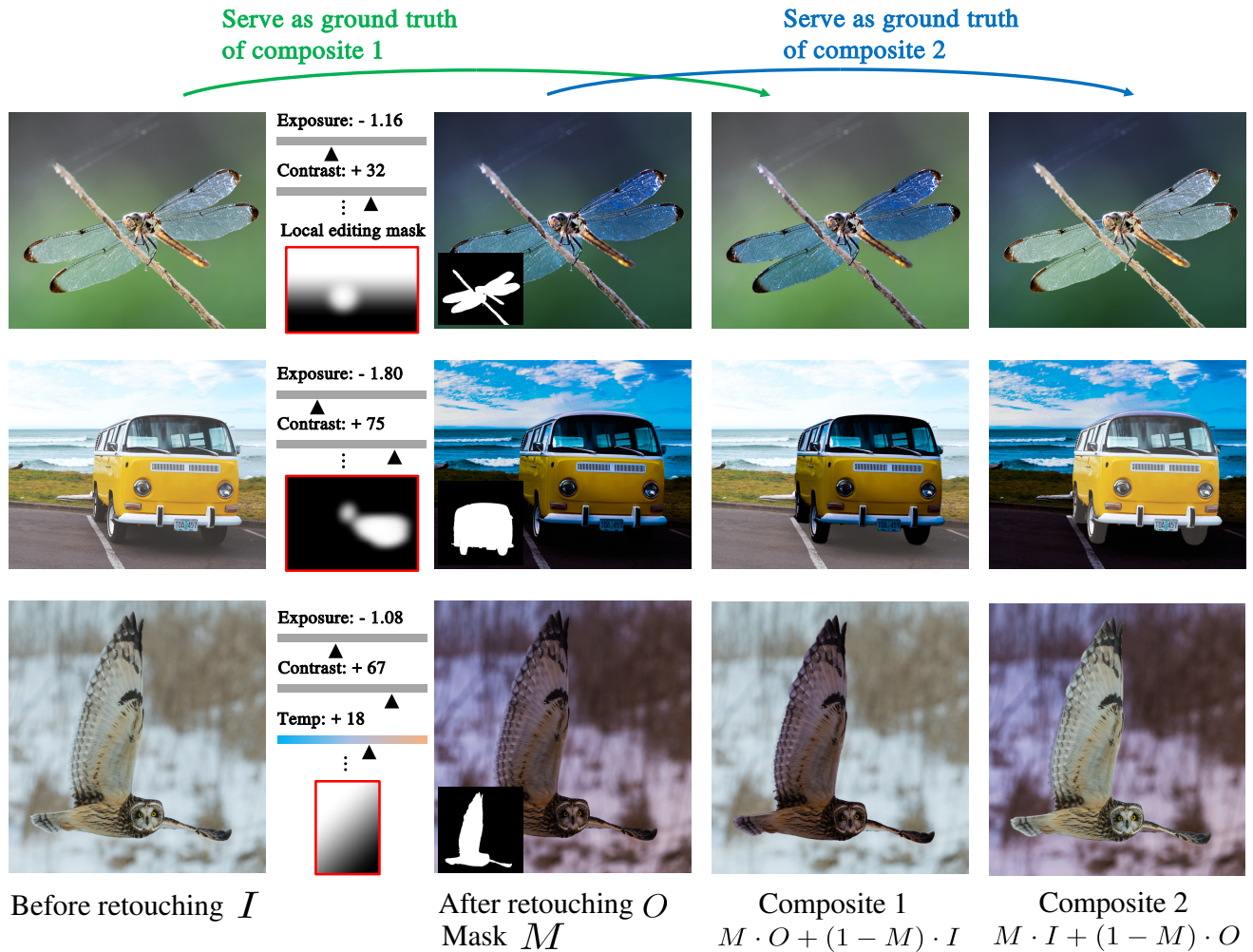


Figure S1. **Construction of Artist-Retouched dataset.** Artist-Retouched dataset contains before/after artist-retouching image pairs $\{I_i, O_i\}_{i=1, \dots, n}$ with the foreground mask M_i for each pair. Artist retouching procedures include both global luminosity/color adjustments as well as local editing. Local editing masks (images with red borders) in the figure indicate the selective regions where artists perform local editing (e.g., shading). Two composite images (Composite 1 and 2) are created and used for training from each pair of images. Unedited image I and retouched image O serve as the ground truth for composite 1 and 2, respectively.

Method	HCOCO		Adobe5k		HFlickr		Hday2night		Entire dataset	
	PSNR \uparrow	SSIM \uparrow	PSNR \uparrow	SSIM \uparrow	PSNR \uparrow	SSIM \uparrow	PSNR \uparrow	SSIM \uparrow	PSNR \uparrow	SSIM \uparrow
Composite	33.92	0.9862	28.51	0.9563	28.44	0.9638	34.32	0.9741	31.74	0.9748
DovNet [4]	35.76	0.9875	35.05	0.9733	30.68	0.9711	34.83	0.9707	34.97	0.9812
IHT [9]	38.38	0.9924	37.02	0.9819	32.84	0.9810	36.79	0.9763	37.33	0.9877
Harmonizer [14]	38.77	0.9936	38.97	0.9888	33.71	0.9833	37.96	0.9813	38.25	0.9909
Ours	39.07	0.9940	38.53	0.9835	33.60	0.9793	38.15	0.9817	38.30	0.9891

Table S1. **Quantitative comparisons on subsets of iHarmony benchmark [4]** at 256×256 resolution. We compare our method with DovNet [4], IHT [9], Harmonizer [14]. PSNR and SSIM are used as metrics. **Red**, and **Blue** correspond to the first and second best results. \uparrow means higher the better, and \downarrow means lower the better.

Visual comparisons on iHarmony benchmark

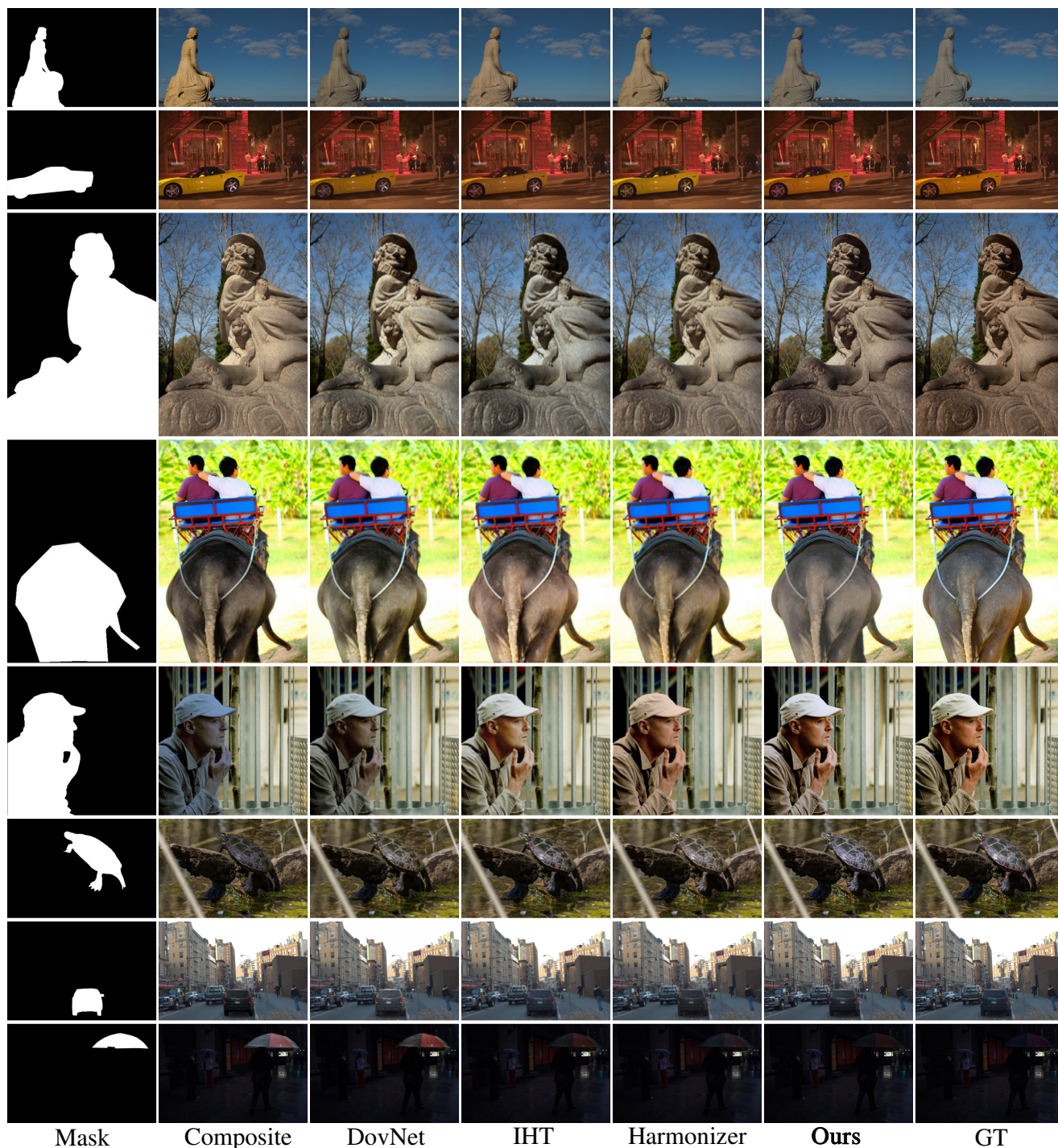
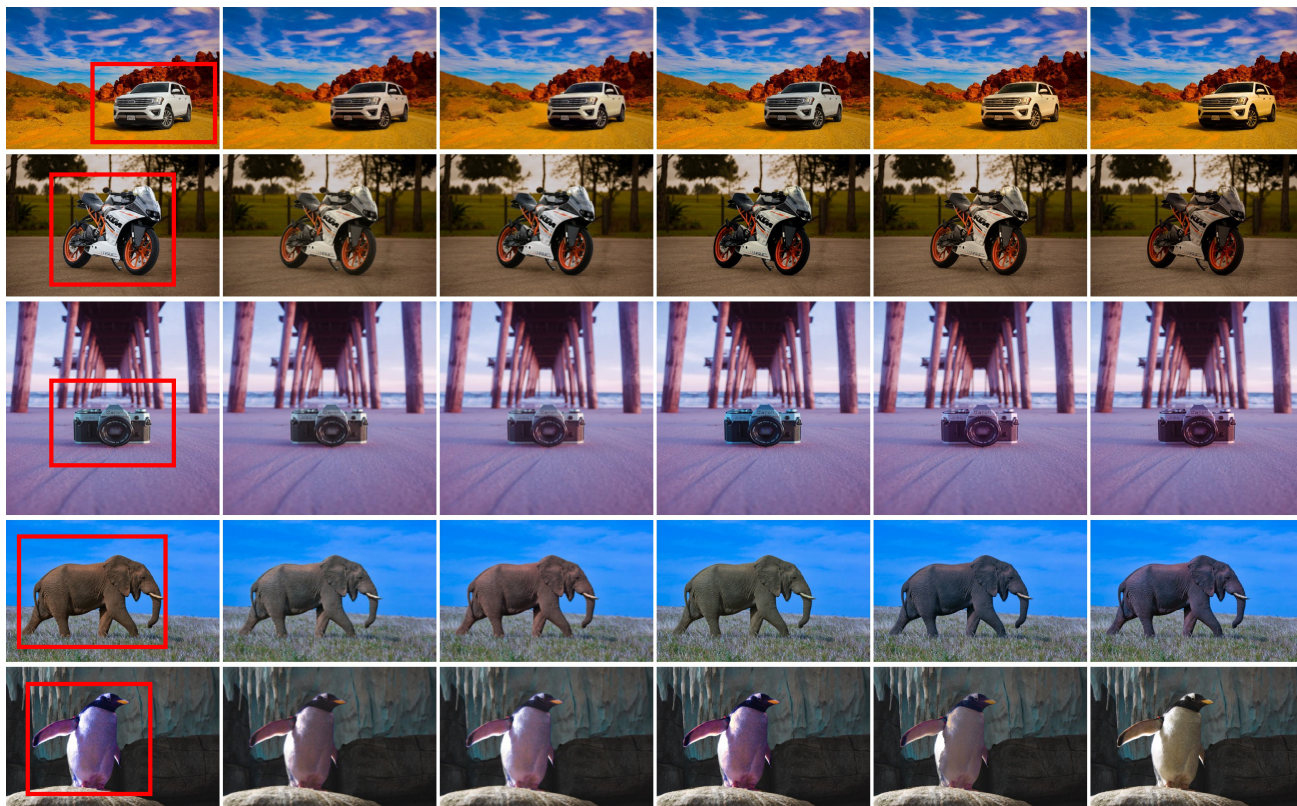


Figure S2. **Representative visual comparisons between state-of-the-art harmonization methods on iHarmony benchmark.** We compare our method with composite image, DovNet [4], IHT [9], Harmonizer [14], and ground truth. Foreground masks are displayed in the first column. For better visualization, we resize the images to the original aspect ratio. Our method shows better visual alignment with the ground truth images than other state-of-the-art methods.

Visual comparisons on *Artist-retouched* dataset



Failure example



Figure S3. **More visual comparisons between state-of-the-art harmonization methods on *Artist-Retouched* dataset.** We compare our method with composite image, DovNet [4], IHT [9], Harmonizer [14], and ground truth. Red boxes indicate the foreground mask of the composite images. Our method shows better visual alignment with the ground truth images compared to other state-of-the-art methods. We also present one failure example, where all methods fail to recover the ground truth appearance, though some of them look harmonious without referring to the ground truth.

Visual comparisons on RealHM benchmark

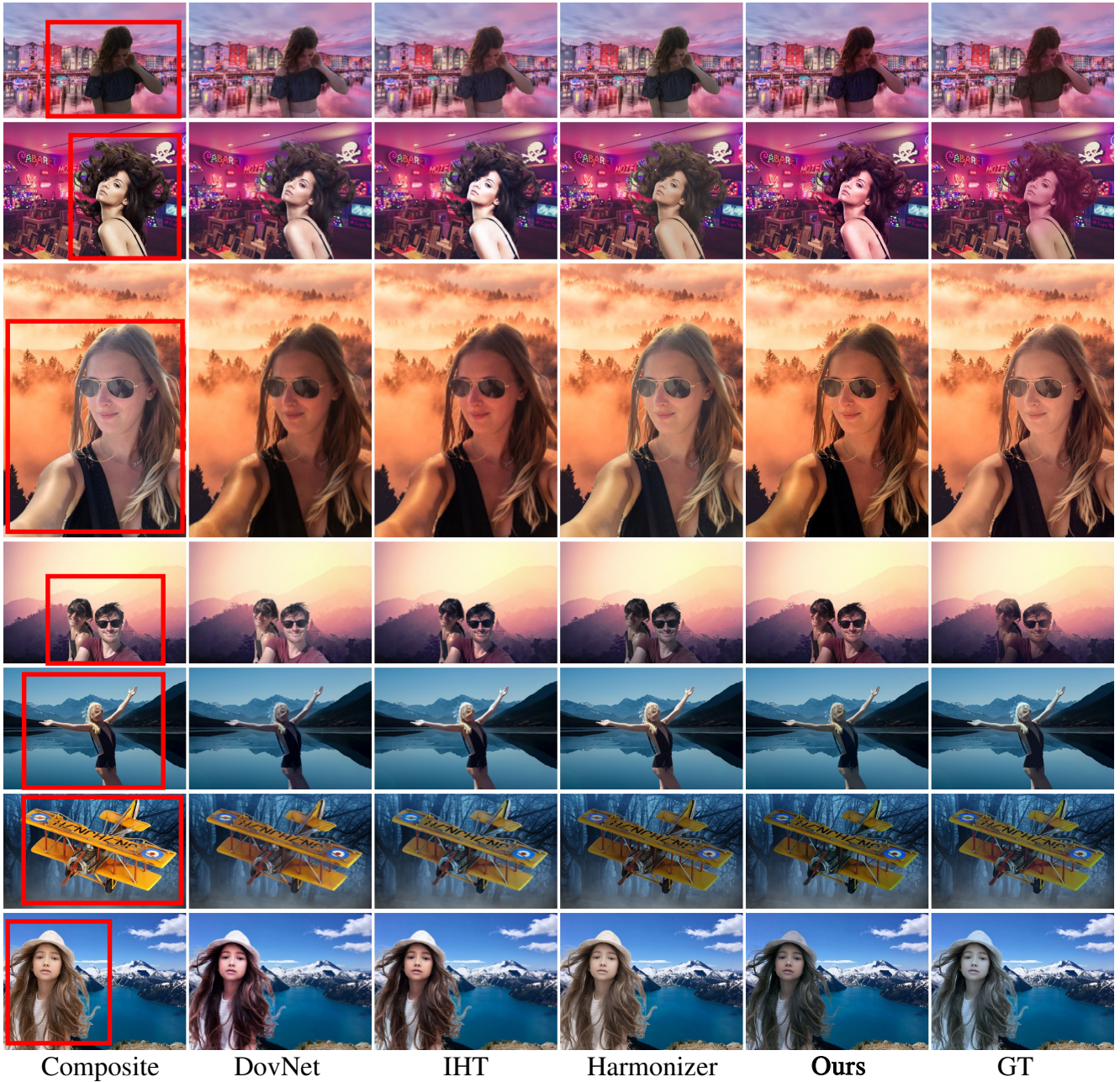


Figure S4. **More visual comparisons between state-of-the-art harmonization methods on RealHM benchmark.** We compare our method with composite image, DovNet [4], IHT [9], Harmonizer [14], and ground truth. Our method shows better color consistency with the ground truth images (row 1, 2, 4, 6, and 7) and deliver more harmonious results.

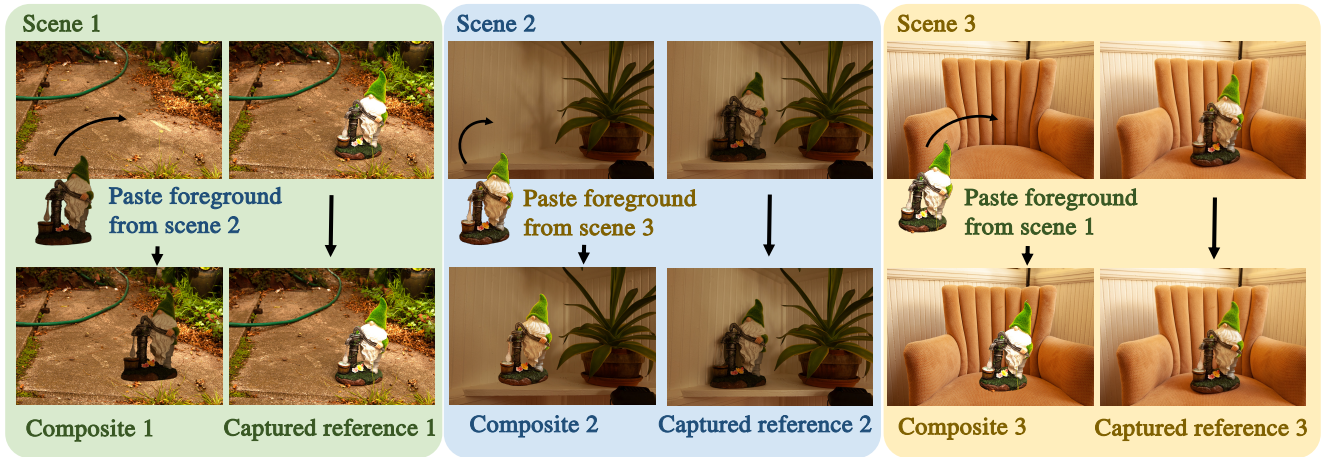


Figure S5. **Construction of composite images with captured reference.** First, we capture the same foreground object against multiple backgrounds (3 backgrounds in the figure), as well as the corresponding "background-only" photos. We then segment the foreground object from one photo and paste it onto the "background-only" image of another to generate the composite images. The captured photo of the same object in the same background scene serves as qualitative references (Here, captured references 1, 2, and 3).

Harmonization results on real composite with captured reference

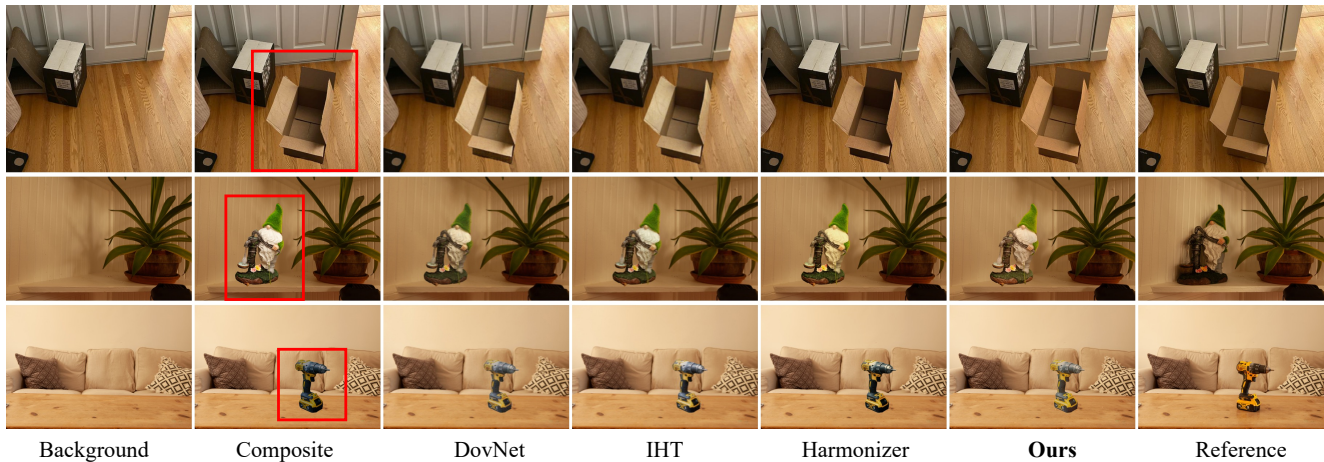


Figure S6. **Real composite harmonization results with captured reference.** The composite is obtained by pasting the foreground object from a different photo (not shown) onto the background (left). The reference (right) is obtained by physically placing the foreground object in the background scene and taking a photo. We compare our method with composite image, DovNet [4], IHT [9], Harmonizer [14], and the captured reference.

Visual comparisons on real composite images

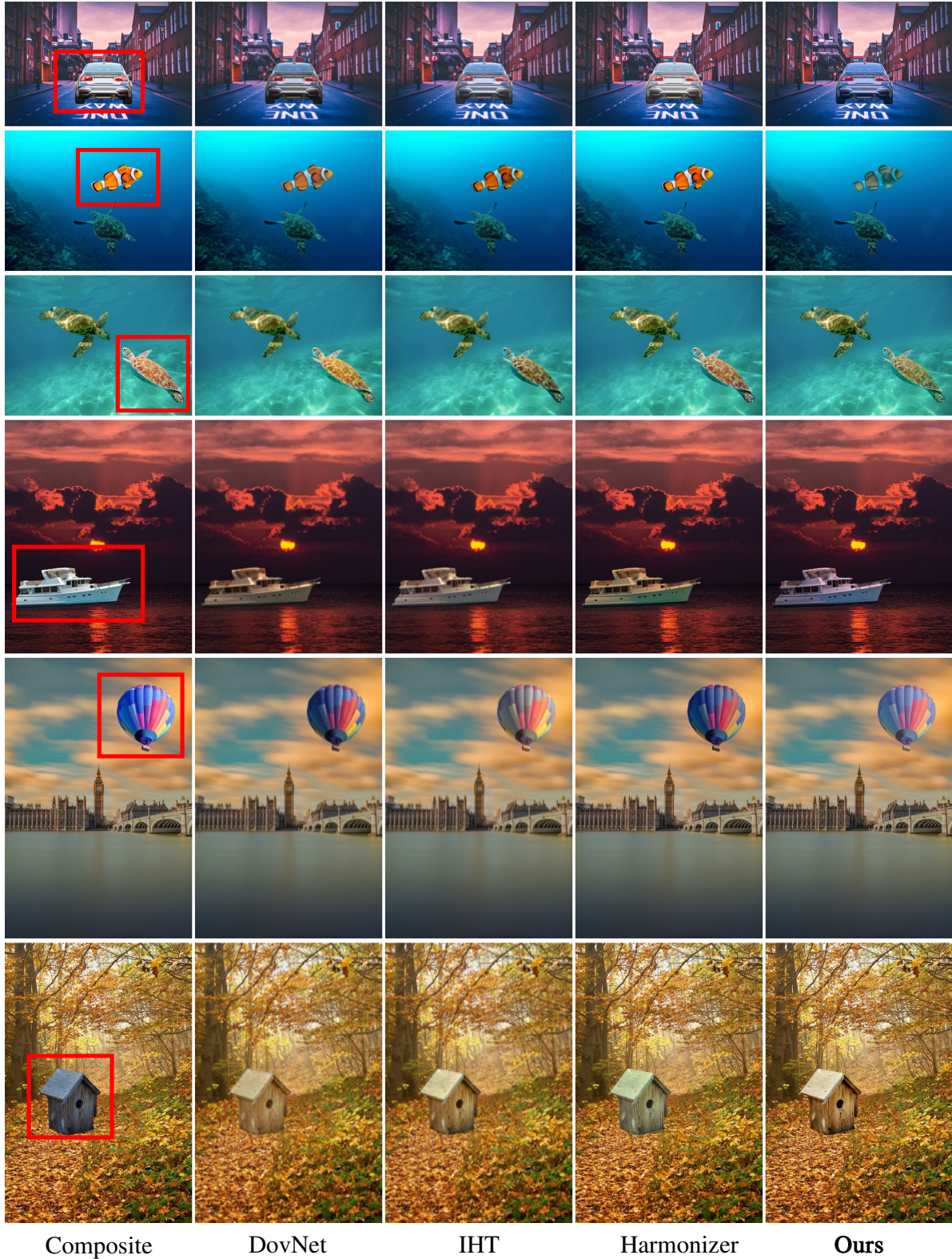


Figure S7. More visual comparisons on real composite images. We compare our method with composite image, DovNet [4], IHT [9], and Harmonizer [14].

Intermediate results and parametric outputs

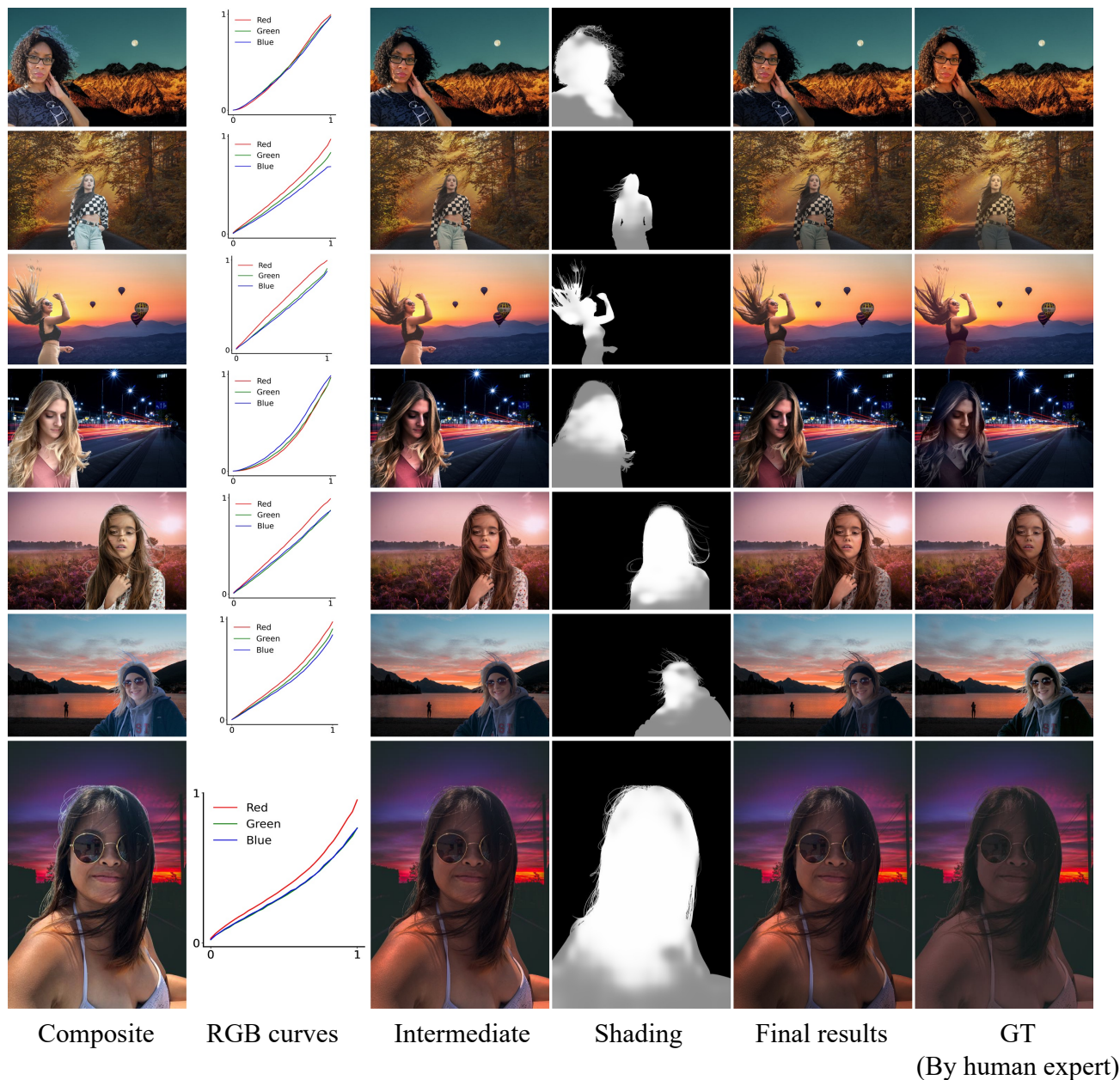


Figure S8. **Intermediate results and parametric outputs on RealHM benchmark.** RGB curves harmonize the global color/tonne (third column), while our shading map corrects the local shading in the final harmonization outputs (fifth column). Our local shading maps agree well with the local shading operations done by human experts/artists (right column).